Proceedings of the 2022 IEEE
International Conference on Robotics and Biomimetics
December 5-9, 2022, Xishuangbanna, China

Generative Design of XingT, A Human-sized Heavy-duty Bipedal Robot

Yizhao Qian, Peiyu Yang, Weicheng Liu, Shuangyuan Sun, Mengyin Fu and Wenjie Song*

***Abstract*— In order to serve humanity better in the disabled assisting, transportation, rescue, and other aspects, a human-sized bionic bipedal structure with low inertia and high-load capacity is presented. The designed robot named XingT adopts a non-coaxial five-link leg structure, after kinematic modeling analysis and structural comparison, being able to bear a load beyond its weight. Besides, bionic tibia modules and passive compliant units are adopted, effectively absorbing motion impact in high-load and strong-impact scenarios. In addition, with structural design and simulation analysis, the proposed five-link structure can realize multi-mode switching, which can adapt to high load application in the convex five-link form and switch to concave five-link mode for light and flexible walking effect. Results of prototype and simulation experiments showed that it can reduce impacts by 67% and increase the load performance by 22.3%, which verifies its structural performance for future practical application.**

I. INTRODUCTION

Modern society is designed to facilitate human production based on human size and physiology. Human beings are not the most powerful, nor the most flexible, but the most suitable labor force for industrial systems and service applications in modern society. The bipedal structure is easier to be accepted by human society because its action mode is similar to human's. However, to have practical application effects, it requires human-sized robots have high load capacity and high flexibility.

The robot must achieve structural innovation to operate efficiently in the environment where humans live and carry a sufficient amount of load. Atlas [1], [2] by Boston Dynamics, caught public's attention when it was announced. Its excellent athletic ability allows it to perform complex maneuvers such as backflips and parkour. Cassie [3], [4] by Agility Robotics is a commercial robot for service purposes. Its linkage mechanism reduces the inertia of legs greatly.

Most bipedal robots are concerned with the dexterity of the robot. ASIMO [5], [6] consists of 26 degrees of freedom including the head, arms, torso, legs and other parts, which can complete various tasks such as climbing stairs. ATRIAS [7]–[11] is a parallel leg robot by OSU. Meanwhile, the upper legs are fitted with spring plates to absorb shocks, making ATRIAS more energy efficient. SLIDER [12], [13] is a bipedal robot with prismatic joint. It has no motor in knees (even no knees), which enabling it to walk without bending knees and reducing manufacturing costs.

This work was partly supported by National Natural Science Foundation of China (Grant No. 61903034, U1913203), Program for Changjiang Scholars and Innovative Research Team in University (IRT-16R06, T2014224), Beijing Institute of Technology Research Fund Program for Young Scholars.

The authors are with School of Automation, Beijing Institute of Technology, Beijing 100081, China.

*Corresponding author: Wenjie Song (email: songwj@bit.edu.cn).

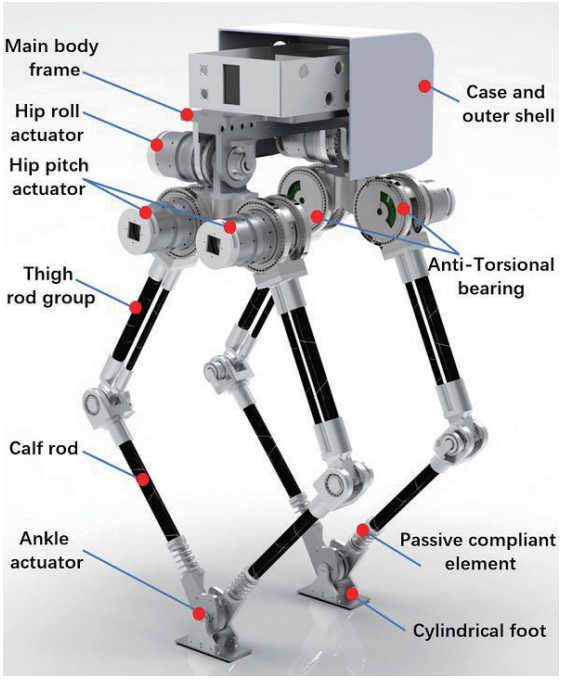

Fig. 1: The human-sized heavy-duty bipedal robot XingT.

Although existing bipedal structures didn't take much load capacity, we can still find inspiration in the high-load multi-legged robots. Bigdog [14] is a quadruped robot used for the carriage of the wild. Bigdog has four actuators on one leg, with the motor closest to the ground to ensure that the ground impact in the same direction with the spring. LLAMA [15] is an electrically driven quadruped robot with a load capacity of 25kg. LLAMA's single leg adopts a coaxial four-bar structure, which demonstrated the load-bearing advantages of parallel structures.

Inspired by these robots, we designed XingT as shown in Fig. 1, a human-sized, electrical motor-driven, form-switchable parallel bipedal robot for high-load missions. It has 8 joints with 4 degrees of freedom (DoF) and a group of five-link made of carbon fiber reinforced polymer at each leg, enabling bring it low-inertia and heavy-loadable capacity. Contributions of our work are listed as follows:

- Propose, model and assemble a new biped structure with low inertia and high-load capacity, which is superior to traditional structure in motion and statics performance. (Section II and Section III (A)(E)(F)(G))
- Propose concave mode of five-link structure, which can switch from convex mode and has advantages in lateral force and space occupying. (Section III (B))
- The passive compliant unit is designed to reduce the

2022 IEEE International Conference on Robotics and Biomimetics (ROBIO) | 978-1-6654-8109-0/22/$31.00 ©2022 IEEE | DOI: 10.1109/ROBIO55434.2022.10011733

Authorized licensed use limited to: TU Delft Library. Downloaded on August 20,2024 at 13:11:41 UTC from IEEE Xplore. Restrictions apply.

foot contact force by about 50.3%, and the new force measurement method is proposed to reduce the cost of force measurement. (Section III (C)(D))

II. Design Theory of the Robot

To determine the leg kinematics and dynamics parameters, this chapter firstly selects the appropriate leg topology and compares it with the representative leg structures. Then we modeled the leg structure.

A. Comparison of representative leg structure

The comparison is made in the following two aspects: firstly, lower the **leg inertia** of the leg structure, the better the movement performance of the robot. Secondly, the higher the leg structure **force transmission index** is, the better the performance of the topology manager is.

The symmetrical five-link structure adopted by XingT has advantages in leg inertia. Many excellent bipedal robots are designed with serial structure, which is similar to the human's leg, but the large inertia of leg raises challenges to its motion stability. In this passage, the author analyses distances between leg center of mass (CoM) and body center of mass in different structures and the inertia of those legs. Although the leg mass of the five-link structure is slightly larger than the series structure, the leg inertia and the position of the leg center of mass are much smaller than the series structure (inertia and CoM position are reduced by 55.9% and 60.5%, respectively), shows that the five-link structure is more flexible than the traditional structure.

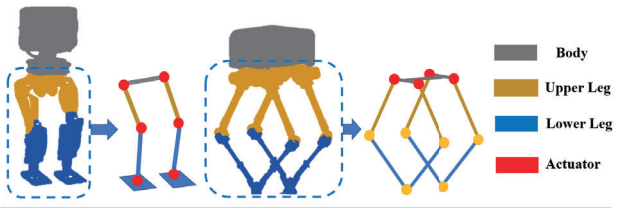

	Total mass	Leg Inertia	COM of the leg
Serial structure	7.152 Kg	0.918 kg*m^2	0.38m under hip
Five-link structure	8.820 Kg	0.404 kg*m^2	0.15m under hip

Fig. 2: Series structure and five link structure and their mass distribution.

The force transmission performance of the three representative structures is shown in Fig. 3. In Fig. 3, a vertical force of 1000N is applied to the foot, and the static performance of the structure is verified by comparing the torque of the motor (**the larger of the two motor torques determine the capacity of the structure**). The calculation results show that the load capacity is 22.3% higher than that of the series structure and 13.0% higher than that of the four-link structure, which shows the advantages of the five-link structure in statics.

B. modeling of five-link structure leg

Leg structure of robot XingT (shown in Fig. 4(a)) is a 3-DOF parallel mechanism, with two actuators at either side

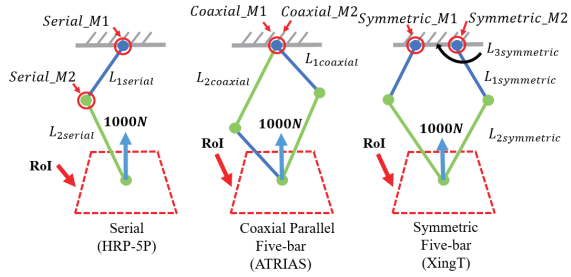

	1	2	3
Motor 1	109.9Nm	241.8Nm	214.0Nm
Motor 2	261.8Nm	221.7Nm	214.0Nm

Fig. 3: Comparison of load performance of different structures. In this experiment, the foot is assumed to move only in the region of interest (RoI), and the average motor torque required to make the foot produce 1000N along the Z-axis in the RoI is given in the table. **Rod's length and RoI are defined in appendix**.

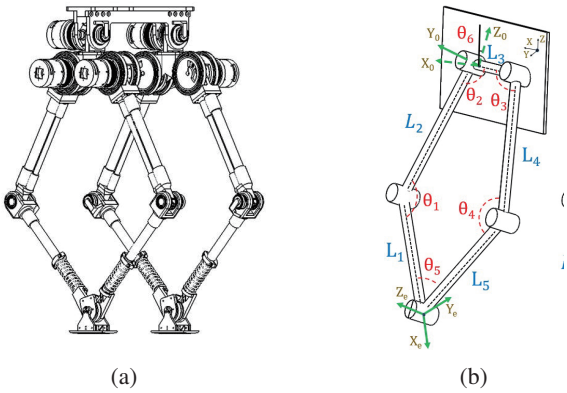

(a) (b)

Fig. 4: Robot and its symbolic definition. (a) Robot XingT. (b) Parameters definition.

of the hip. The parameters and symbols used are shown in Fig. 4(b).

Closed chain structure usually use numerical methods to solve their kinematic equations. The cost function are expressed as follows:

$$
\begin{aligned}
&\theta_6 = arctan\left(\frac{f_y}{f_z}\right)\\
&C = C_{x,l} + C_{x,r} + C_{y,l} + C_{y,r}\\
&C_{x,l} = (f_x - h_x)^2 - ((L_2 * c_2) + (L_3/2 - L_1 * c_{2,1})))^2\\
&C_{x,r} = (f_x - h_x)^2 - ((L_4 * c_3)) + (L_3/2 - L_5 * c_{4,3})))^2\\
&C_{z,l} = (f_y - h_y)^2 + (f_z - h_z)^2 - ((L_2 * c_2)) - (L_1 * c_{2,1})))^2\\
&C_{z,r} = (f_y - h_y)^2 + (f_z - h_z)^2 - ((L_4 * c_3)) - (L_5 * c_{3,4})))^2
\end{aligned}
\tag{1}
$$

Where, f_x, f_y, h_x and h_y represents the X and Y coordinate of the foot and hip. c_i and $c_{i,j}$ represents $cos(\theta_i)$ and $cos(\theta_i + \theta_j)$ respectively. θ_2 and θ_3 is solved numerically by minimize C. θ_6 solved by the first equation.

The Jacobian is obtained by taking the derivative of eq1

Authorized licensed use limited to: TU Delft Library. Downloaded on August 20,2024 at 13:11:41 UTC from IEEE Xplore. Restrictions apply.

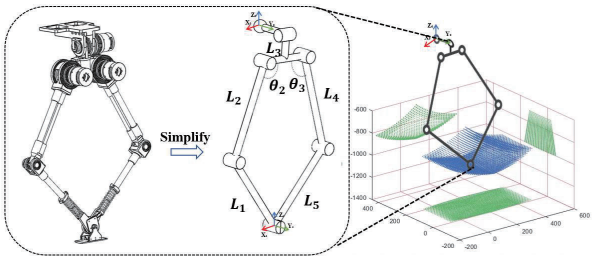

Fig. 5: Overview of the leg workspace, including 3D view and 3D projection view.

with $\dot{\theta}_6$, $\dot{\theta}_2$, and $\dot{\theta}_3$, which is a 6 by 3 matrix as follows:

$$\mathbb{J}_{6\times3}(\theta) = \begin{bmatrix} T_{3\times3} \\ \Omega_{3\times3} \end{bmatrix} \tag{2}$$

The workspace of non-coaxial five-link structure is shown in Fig. 5.

III. Mechanical Design

A. Design overview

The mechanical structure of XingT includes hip joint generator, leg linkage system, body frame and other structures. It has a total of 8 DoFs and each leg is equipped with 4 motors. Fig. 6 shows the operating and physical parameters of the robot. The CoM of one leg is located 12cm below the hip joint. Its frame structure is made of 6061 aluminum alloy, and carbon fiber rods are used as stress components for both legs. The length and structural parameters of each rod are shown in the figure following.

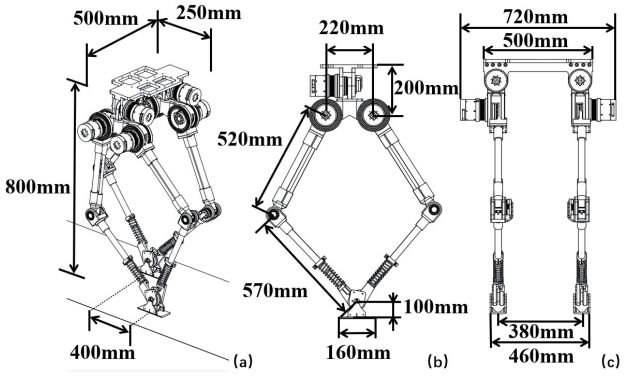

Fig. 6: (a) Dimension parameters in working mode of XingT. (b, c) Physical parameters of XingT.

B. Multimodal design

The convex five-link structure has two disadvantages: large space occupation and low lateral force capacity, which can be solved by using the concave five-link structure. Fig. 7 shows the workspace problems of several typical leg structures. XingT can switch between concave and convex mode (Fig. 7(c) and (d)) by multi-solution of five-link structure. In this chapter, the kinematics and mechanical properties of the concave five-link structure are analyzed and compared with the convex five-link structure. The leg structure switching process and the concave five-link gait verification experiment are shown in next section.

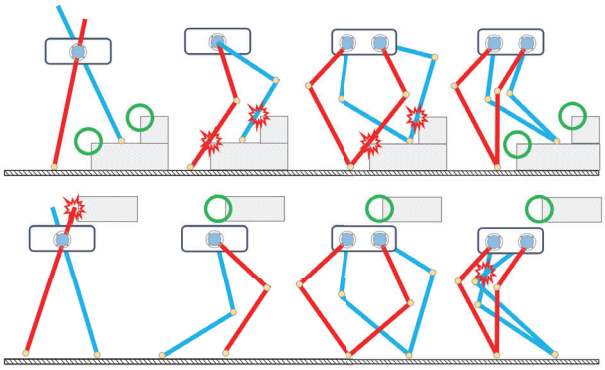

Fig. 7: Comparison of typical leg structures and five-link structures in passing ability.

Fig. 8 shows the torques of motors when gravity and friction are applied to the footpoint when they move in RoI. The result shows that the concave five-link structure can reduce the motor torque (total torque of motor is small in Fig.8) and avoids unbalanced motor output (unbalanced means one motor is in high torque while the other is in low)

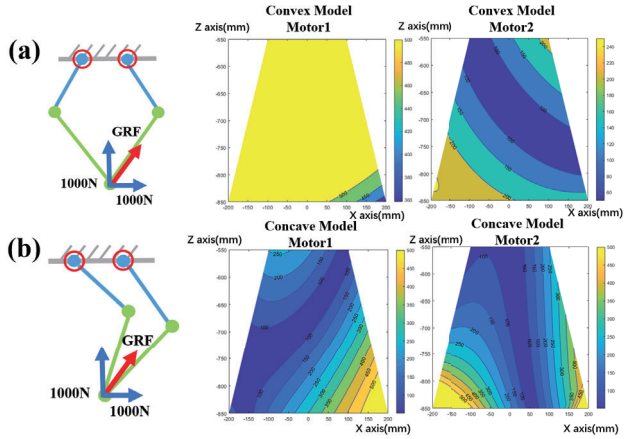

Fig. 8: Motor torque at 1000N in X-axis direction and 1000N in Z-axis direction in RoI. In this figure, the trapezoidal regions are RoI, and the color of each point in the trapezoidal represents the motor torque when the foot is at that point.

The space occupation of the leg structure can be used to evaluate robot passing capacity in complex environments. The occupied area of series structure, coaxial five-link structure, convex five-link structure, and concave five-link structure is $0.207m^2$, $0.383m^2$, $0.428m^2$, $0.255m^2$ respectively. The space occupation of concave five-link mode is reduced by 40.4% compared with convex five-link mode.

C. Compliance structure design

Passive compliance design is an approach for controlling the contact forces between a robotic leg and a stiff environment. By using elastics components such as springs or dampers, GRF (Ground Reaction Force) will occur as desired and reduce disturbance when walking. The experiment in

Authorized licensed use limited to: TU Delft Library. Downloaded on August 20,2024 at 13:11:41 UTC from IEEE Xplore. Restrictions apply.

section IV proves the effectiveness of the passive compliance scheme.

As shown in Fig. 9, the symmetrical five-link structure is used in compliant control to reduce GRF, which is always propagates along the axial direction of the lower leg [7] in parallel leg structure, as shown in Fig. 9(c). Therefore, by a pair of elastic elements on the lower leg, preventing GRF from being directly transmitted to the robot body becomes possible.

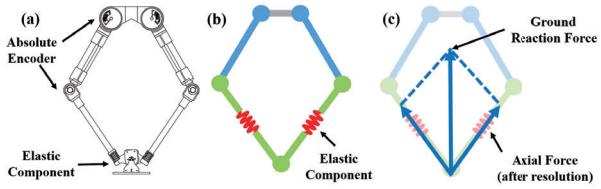

Fig. 9: Structure of passive compliance. (a) Mechanical structure. (b) Simplified model. (c) GRF propagation in lower leg.

Fig. 10 shows the structure of the compliance component in which the lower leg rod and wellfeder wave springs are used as compliant component. To prevent damage to the spring when stretching and low control accuracy due to low elastic force when the spring is near its original length, precompression is adopted to make the spring have the preloading force and always remain in a compression state.

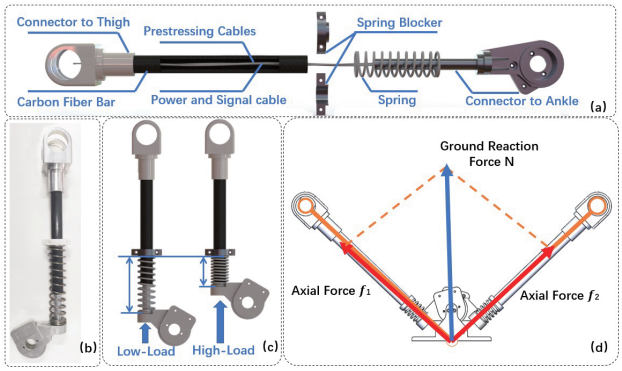

Fig. 10: (a) Structure of lower leg. (b) Prototype. (c) Compression deformation of the leg. (d) GRF decomposition.

D. Method of GRF measurement

After GRF deforms the spring, the leg configuration modifies due to the change in lower leg length, which makes it possible to measure GRF by measuring the leg configuration change. GRF is traditionally measured by multiaxial force sensors and their amplifiers which are expensive and large in size. In this paper, angle sensors placed on two knee joints and motors are used to measure the inner angle of the five-link structure to calculate the GRF. Fig. 11(b) is the comparison of GRF and the value obtained by deformation. The result shows that the average error is 2.3%. **The active compliance test in section IV adopts this force measuring method and achieves stability control**.

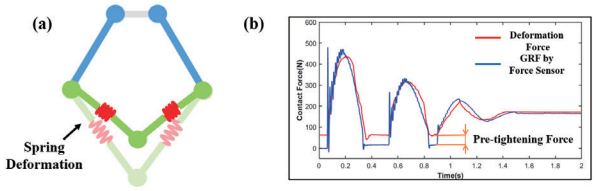

Fig. 11: GRF measurement. (a) Deformation under the GRF. (b) Comparation Force sensor based on deformation and actual GRF measured by force sensor.

E. Design of Integrated Drive Unit

The actuator of the bipedal robot XingT is mainly composed of a frameless torque motor and harmonic reducer. The motor has a rated torque of 1.44Nm, stall torque is 4.66Nm, and a maximum speed of 2950rpm. Fig. 12 shows the physical picture of the high-torque motor. Motor driven by ELMO gold driver and the stall torque is 298Nm through a customized harmonic reducer. An encoder is installed at the motor to record its position and speed. The total weight of the actuator is 2.4kg, which is a lightweight and high-torque integrated drive unit [15].

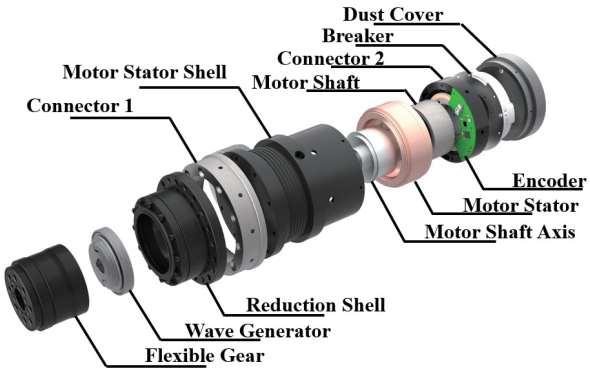

Fig. 12: The inner structure of integrated drive unit.

F. Load-bearing structure design

Non-coaxial five-link linkages structure is the core of load capacity. XingT's upper leg imitated the tibial structure, shown in Fig. 13. The leg joint is made of aluminum alloy, and leg skeleton is made of carbon fiber bar. Fig. 13(d) and 13(e) respectively show the stress of bionic and single-rod structures when receiving constant torque and force. The bionic structure weighs about 354g and its stress peak is 124Mpa, while the single-rod structure weighs about 391g and its stress peak is 155Mpa, indicating that the bionic structure has advantages both in reducing weight and enhancing structural strength.

G. Walking control and sensor configuration

In Section IV II, LIPM model is used for XingT to walk stably. LIPM model disregards leg mass in the walking process, which is suitable for XingT with slight inertia

Authorized licensed use limited to: TU Delft Library. Downloaded on August 20,2024 at 13:11:41 UTC from IEEE Xplore. Restrictions apply.

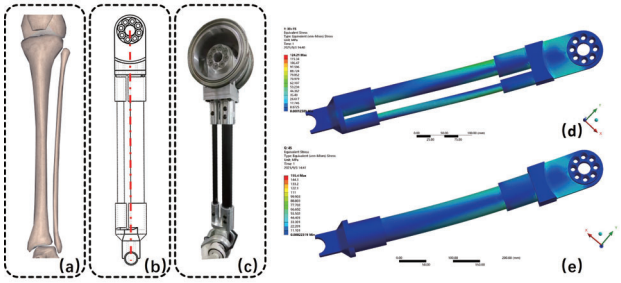

Fig. 13: (a) Skeletal diagram of tibia and fibula. (b) The schematic diagram of the mechanical structure. (c) Prototype. (d) Finite element analysis results of 30mm + 15mm bar. (e) Finite element analysis results of 45mm bar.

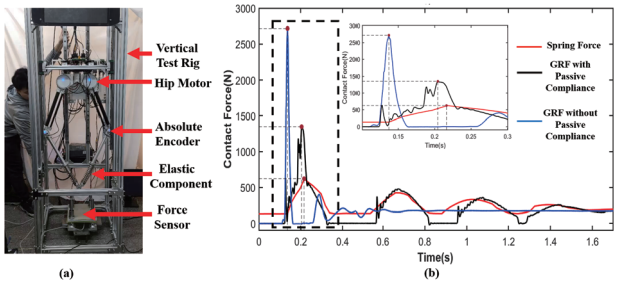

Fig. 14: Result of Passive compliance experiment. The leg structure is droped from 54cm height. (a) Vertical test rig and leg structure. (b) Contact forces with and without passive compliance.

legs. Before walking, the robot calculates the trajectory of footpoint and CoM offline and controls the robot to track the trajectory online through MPC+PID during walking to make the robot walk stably

XingT uses Xense® MTI-30 and BenWake® TF-03 to measure its attitude and position. The ZeroErr® e-18 absolute encoder and HBM® U93-B2083 force sensor are equipped to measure GRF by the method proposed above and determine whether the robot is landed on the ground.

IV. Experiment and Results

We built a physical prototype to verify the workspace and mechanical characteristics of the leg structure. In addition, the bipedal gait of the whole machine was verified by simulation method.

A. Experiment of Mechanical Structure

For the single-leg experiment, the symmetric five-link leg structure is constrained on a 1-DoF vertical test rig using four sliding rails. Electronics and power are mounted off-board currently. Payload is about 6.5kg set on the leg including sliders, onboard trusses, and fasteners.

a) Experiment of passive compliance

Great passive compliance is the premise of increasing maximum load and robustness. In this experiment, The leg falls from 54cm height with and without passive compliance. Fig. 14 shows passive compliance reduces the impact by about 50.3%.

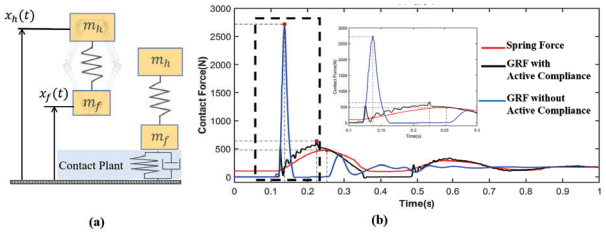

Fig. 15: Result of active + passive compliance experiment. (a) Model of VMC. (b) Contact forces with and without active+passive compliance.

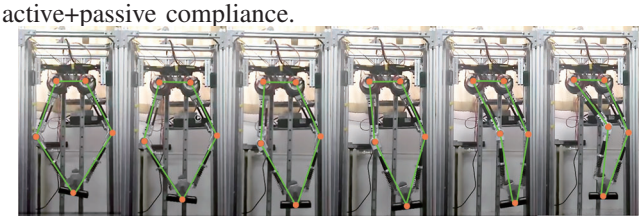

Fig. 16: Trajectory of leg in mode switching.

b) Experiment of active and passive compliance

Virtual model control (VMC) is an algorithm to realize active compliance [16]. VMC creates a virtual spring and damper between hip and ground. In this experiment, Prototypes with VMC algorithms were dropped from 54cm. Fig. 15 shows the impact with only passive compliance and active + passive compliance. Compared with the results of no compliance, active compliance reduced the foot impact force by 67%.

c) Mode switching experiment.

In the narrow terrain, the robot's movement area is limited. XingT uses the characteristic of five-link structure to reduce the space occupied by the robot to achieve narrow space. Fig. 16 shows the trajectory of leg structure in mode switching.

B. Simulation and prototype experiment

Bipedal robots usually have basic gaits as the reference track of the foot. XingT with five-link parallel leg structure is suitable for the generation of its gait by inverted pendulum model, that's due to the distance between CoM and the center of hip is very close. In this paper, XingT is capable of walking and executing other tasks.

XingT performs several experiments in simulation. Fig. 17(a) shows the gait verification of the robot, and the robot walks according to the pre-calculated gait. Fig. 17(b) shows the robot's mode switching process. Fig. 18(a)-(f) shows the robot's walking process. In this plain walking experiment, XingT walked 6.7m from a standstill within 6 seconds, with an average speed about 1.12m/s.

V. CONCLUSIONS

In this work, we present a human-sized bionic bipedal robot XingT, which adopts a non-coaxial five-link leg structure to get the low inertia and high-load capacity through kinematic modeling analysis and structural comparison. A high energy density integrated drive unit was designed as the driver to complete high-load tasks. Results show that the

Authorized licensed use limited to: TU Delft Library. Downloaded on August 20,2024 at 13:11:41 UTC from IEEE Xplore. Restrictions apply.

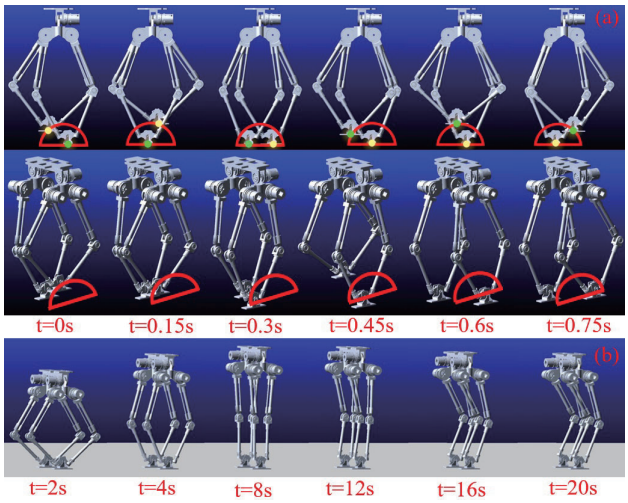

Fig. 17: Simulation experiments. (a) Walking gait. (b) Mode switching process.

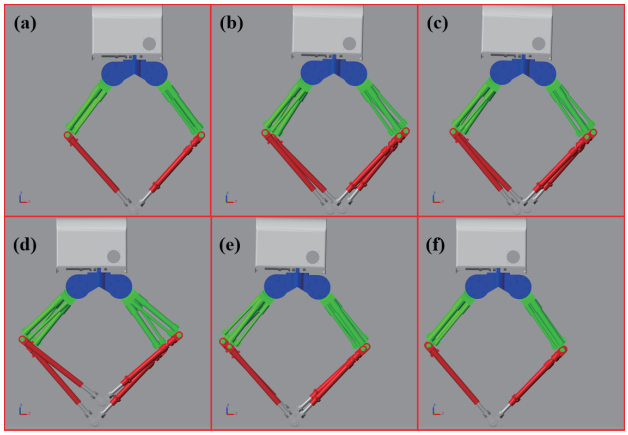

Fig. 18: Simulation of walking experiments. (a)-(f) shows different sections of walking.

five-link leg structure was increased by 22.3% compared with traditional serial structures. Besides, jumping from a height of 54cm with a load of 6.5kg, its foot impact is reduced by 67%, which proved its good passive compliance. And the walking gait and multi-mode switching were also tested and verified in prototype and simulation experiments. In the future, we plan to work on stability control for unassisted 3D walking.

REFERENCES

[1] S. Feng, E. Whitman, X. Xinjilefu, and C. G. Atkeson, "Optimization based full body control for the atlas robot," in *2014 IEEE-RAS International Conference on Humanoid Robots*. IEEE, 2014, pp. 120–127.

[2] B. Dynamics, "What's new, atlas?" https://www.youtube.com/watch?v=fRj34o4hN4I, accessed September 13, 2021.

[3] X. Xiong and A. D. Ames, "Bipedal hopping: Reduced-order model embedding via optimization-based control," in *2018 IEEE/RSJ International Conference on Intelligent Robots and Systems (IROS)*. IEEE, 2018, pp. 3821–3828.

[4] O. S. University, "Cassie - next generation robot," https://www.youtube.com/watch?v=Is4JZqhAy-Mt=99s, accessed September 13, 2021.

[5] J. Chestnutt, M. Lau, G. Cheung, J. Kuffner, J. Hodgins, and T. Kanade, "Footstep planning for the honda asimo humanoid," in *Proceedings of the 2005 IEEE international conference on robotics and automation*. IEEE, 2005, pp. 629–634.

[6] Y. Sakagami, R. Watanabe, C. Aoyama, S. Matsunaga, N. Higaki, and K. Fujimura, "The intelligent asimo: System overview and integration," in *IEEE/RSJ international conference on intelligent robots and systems*, vol. 3. IEEE, 2002, pp. 2478–2483.

[7] D. Renjewski, A. Spröwitz, A. Peekema, M. Jones, and J. Hurst, "Exciting engineered passive dynamics in a bipedal robot," *IEEE Transactions on Robotics*, vol. 31, no. 5, pp. 1244–1251, 2015.

[8] A. Ramezani, J. W. Hurst, K. Akbari Hamed, and J. W. Grizzle, "Performance analysis and feedback control of atrias, a three-dimensional bipedal robot," *Journal of Dynamic Systems, Measurement, and Control*, vol. 136, no. 2, p. 021012, 2014.

[9] S. Rezazadeh, A. Abate, R. L. Hatton, and J. W. Hurst, "Robot leg design: A constructive framework," *IEEE Access*, vol. 6, pp. 54 369–54 387, 2018.

[10] B. G. Buss, A. Ramezani, K. A. Hamed, B. A. Griffin, K. S. Galloway, and J. W. Grizzle, "Preliminary walking experiments with underactuated 3d bipedal robot marlo," in *2014 IEEE/RSJ International Conference on Intelligent Robots and Systems*. IEEE, 2014, pp. 2529–2536.

[11] C. Hubicki, J. Grimes, M. Jones, D. Renjewski, A. Spröwitz, A. Abate, and J. Hurst, "Atrias: Design and validation of a tether-free 3d-capable spring-mass bipedal robot," *The International Journal of Robotics Research*, vol. 35, no. 12, pp. 1497–1521, 2016.

[12] K. Wang, A. Shah, and P. Kormushev, "Slider: A bipedal robot with knee-less legs and vertical hip sliding motion," in *Memorias de Congresos UTP*, 2018, pp. 109–116.

[13] K. Wang, D. Marsh, R. P. Saputra, D. Chappell, Z. Jiang, A. Raut, B. Kon, and P. Kormushev, "Design and control of slider: An ultra-lightweight, knee-less, low-cost bipedal walking robot," in *2020 IEEE/RSJ International Conference on Intelligent Robots and Systems (IROS)*. IEEE, 2020, pp. 3488–3495.

[14] D. Wooden, M. Malchano, K. Blankespoor, A. Howardy, A. A. Rizzi, and M. Raibert, "Autonomous navigation for bigdog," in *2010 IEEE international conference on robotics and automation*. Ieee, 2010, pp. 4736–4741.

[15] J. Nicholson, J. Jasper, A. Kourchians, G. McCutcheon, M. Austin, M. Gonzalez, J. Pusey, S. Karumanchi, C. Hubicki, and J. Clark, "Llama: Design and control of an omnidirectional human mission scale quadrupedal robot," in *2020 IEEE/RSJ International Conference on Intelligent Robots and Systems (IROS)*. IEEE, 2020, pp. 3951–3958.

[16] Z. He, F. Meng, X. Chen, Z. Yu, X. Fan, R. Sato, A. Ming, and Q. Huang, "Controllable height hopping of a parallel legged robot," *Applied Sciences*, vol. 11, no. 4, p. 1421, 2021.

APPENDIX

A. Definition of RoI

Due to the different working spaces of each leg structure, the region of interest (RoI) is defined according to the foot movement trajectory of bipedal robots. RoI is a trapezoid with 200mm upper line, 400mm lower line, and 300mm high.

B. Definition of linkage parameters

TABLE I: Parameters used in the comparison

Param	Value	Param	Value	Param	Value
$L_{1serial}$	0.50m	$L_{2symmetric}$	0.53m	d_{bar}	0.97kg/m
$L_{2serial}$	0.50m	$L_{3symmetric}$	0.22m	m_{stator}	2.4kg
$L_{1coaxial}$	0.40m			m_{shaft}	0.48kg
$L_{2coaxial}$	0.50m			m_{hinge}	0.5kg
$L_{1symmetric}$	0.40m			τ_{max}	$298N \cdot m$

Authorized licensed use limited to: TU Delft Library. Downloaded on August 20,2024 at 13:11:41 UTC from IEEE Xplore. Restrictions apply.